

# Identifiable Multi-View Causal Discovery Without Non-Gaussianity

Ambroise Heurtebise<sup>1\*</sup>, Omar Chehab<sup>2</sup>, Pierre Ablin<sup>3</sup>,  
Alexandre Gramfort<sup>1</sup>, Aapo Hyvärinen<sup>4</sup>

<sup>1</sup>Inria, CEA, University of Paris-Saclay, France

<sup>2</sup>ENSAE, CREST, IP Paris, France

<sup>3</sup>Apple

<sup>4</sup>University of Helsinki, Finland

## Abstract

We propose a novel approach to linear causal discovery in the framework of multi-view Structural Equation Models (SEM). Our proposed model relaxes the well-known assumption of non-Gaussian disturbances by alternatively assuming diversity of variances over views, making it more broadly applicable. We prove the identifiability of all the parameters of the model without any further assumptions on the structure of the SEM other than it being acyclic. We further propose an estimation algorithm based on recent advances in multi-view Independent Component Analysis (ICA). The proposed methodology is validated through simulations and application on real neuroimaging data, where it enables the estimation of causal graphs between brain regions.

## 1 Introduction

Causal discovery is a fundamental problem in scientific data analysis as well as several technological applications [18]. The basic problem is that we are given a number of observed variables, and we need to infer or learn which variables cause which, and with what “connection strengths”. In the typical case, we only observe the data passively without any possibility of performing interventions, and this purely observational quality of the data makes the problem difficult.

Typically, the problem is formalized as a structural equation model (SEM) [2], also called a functional causal model. Then the question is how to estimate the SEM using statistical theory. In fact, before even considering estimation methods, we need to know if it is at all possible to solve the problem. This is the question of *identifiability* of the model: can the parameters that describe the causal relations and directions be (uniquely) estimated?

A well-known fact is that if all the variables are Gaussian, the model is *not* identifiable without further strong assumptions. The literature proposes different kinds of further assumptions to actually enable identifiability. Some of the earliest work showed the directions can sometimes be recovered by an analysis of the *conditional independencies* [28]; however, this is only possible in some special cases and notably not possible in the case of observing only two variables. A major advance was to consider a linear model together with *non-Gaussianity* [26], which leads to full identifiability of the model under weak conditions such as notably acyclicity; however, such non-Gaussianity may not be clearly visible in many data sets. A related framework was proposed by assuming that the cause undergoes a *nonlinear transform*, while the disturbance is still additive [10]; however the nonlinearity may not be clearly visible in many applications, and it slightly contradicts the additivity of the disturbance. Further frameworks were proposed by Peters and Bühlmann [17], Zhang and Hyvärinen [32], Monti et al. [15].

Here, we consider the linear, multi-view case, i.e. we assume that several related data sets are observed, and the model is linear. In particular, we assume that the disturbances (also called external influences, or noise) have some shared information among the data sets, but are not identical. The main novelty in our framework is that we show how the multi-view information leads to a new kind of identifiability result: the model is fully identifiable even if all the variables are Gaussian, and without any special assumptions on the structure of the SEM, other than the ubiquitous acyclicity (“DAG”) assumption. To

---

\*Corresponding author [ambroise.heurtebise@inria.fr](mailto:ambroise.heurtebise@inria.fr)

compensate the lack of non-Gaussianity, we do need an assumption that the variances of the disturbances in different views are distinct; thus, it is the variability over views that allows for identifiability. While the multi-view case has been considered by Shimizu [24], he did not consider disturbances with some shared information among the data sets. Furthermore, he only showed how to use the multiple views to improve the estimation, still assuming non-Gaussianity of the disturbances.

We also develop new algorithms for such multi-view causal discovery. These are based on a recent theory of multi-view independent component analysis (ICA) proposed by Richard et al. [20], and they can handle both Gaussian and non-Gaussian disturbances. As a practical application of the methods, we analyze brain imaging data where the different views are data from different subjects under the same stimulation. This sheds light on the causal connections between different brain regions.

## 2 Background

**Causal ordering** In the following, we consider a matrix  $\mathbf{B} \in \mathbb{R}^{p \times p}$  that encodes the structure of a directed acyclic graph (DAG), which means that the non-zero entries of  $\mathbf{B}$  represent the edges of the graph. It follows that there exist a strictly lower triangular matrix  $\mathbf{T}$  and a permutation matrix  $\mathbf{P}$ , referred to as the *causal ordering*, such that  $\mathbf{B} = \mathbf{P}^\top \mathbf{T} \mathbf{P}$ . In general, such an ordering is not unique.

**LiNGAM, a model for causal discovery** Let  $\mathbf{x} \in \mathbb{R}^p$  be a random vector of observations and let  $\mathbf{B} \in \mathbb{R}^{p \times p}$  represent a DAG. We consider a structural equation model, also known as a functional causal model, where the data follows

$$\mathbf{x} = \mathbf{B}\mathbf{x} + \mathbf{s} \quad (1)$$

where the entries  $s_1, \dots, s_p$  of the vector  $\mathbf{s} \in \mathbb{R}^p$  are independent noise terms, called disturbances. Causal discovery consists in inferring the parameters  $\mathbf{B}$  of the model, from observations of  $\mathbf{x}$ . Yet, the identifiability of such a model and therefore the uniqueness of the inferred  $\mathbf{B}$  is not straightforward. In fact, it is well-known that Gaussian noises make the model unidentifiable, in general [22, 6]. A major advance was that Shimizu et al. [26] assumed the noise variables to be *non-Gaussian* leading to their Linear Non-Gaussian Acyclic Model (LiNGAM), which leads to identifiability, as discussed later. In the model, we can then interpret  $\mathbf{P}$  as representing a reordering of the observations, such that the permuted entries  $\mathbf{P}\mathbf{x}$  satisfy

$$\mathbf{P}\mathbf{x} = \mathbf{T}\mathbf{P}\mathbf{x} + \mathbf{P}\mathbf{s} \quad (2)$$

where the causal matrix between the  $\mathbf{P}\mathbf{x}$  is now  $\mathbf{T}$  and thus strictly lower triangular. This means any entry  $(\mathbf{P}\mathbf{x})_j$  is a weighted sum of previous entries  $(\mathbf{P}\mathbf{x})_{<j}$  and noise  $(\mathbf{P}\mathbf{s})_j$ . Because  $(\mathbf{P}\mathbf{x})_j$  does not depend on future entries  $(\mathbf{P}\mathbf{x})_{>j}$ , we say that  $\mathbf{x}$  follows a causal ordering given by  $\mathbf{P}$ .

**Relation of LiNGAM to ICA** The LiNGAM model, or any similar model based on Eq. 1, can be rewritten as a latent variable model, in particular an Independent Component Analysis (ICA) model [11] as

$$\mathbf{x} = \mathbf{A}\mathbf{s} \quad (3)$$

where, again, the entries in  $\mathbf{s}$  are independent and non-Gaussian, and the “mixing” matrix  $\mathbf{A}$  expresses how the data is generated from the latents, and is given by  $\mathbf{A} = (\mathbf{I} - \mathbf{B})^{-1}$ , where  $\mathbf{B}$  is a DAG. Now, many methods developed for ICA can be used to estimate the matrix  $\mathbf{A}$ , but it is important to take this special structure into account [26]. In particular, any ICA algorithm does not directly return the correct matrix  $\mathbf{A}$  but rather a related matrix where the columns of  $\mathbf{A}$  may appear in an arbitrary order.

**Identifiability of LiNGAM** Shimizu et al. [26] showed that the LiNGAM model is identifiable in terms of the matrix  $\mathbf{B}$ , with no indeterminacies unlike in basic ICA. A rigorous re-statement of this result is given in the following theorem which we prove for completeness in Appendix A.2.

**Theorem 1** (Identifiability of LiNGAM) *In the statistical model defined by Eq. 1, the parameter  $\mathbf{B}$  is identifiable, provided that the entries in  $\mathbf{s}$  are mutually independent, that at most one of them is Gaussian, and that  $\mathbf{B}$  is a DAG.*

A further question that has received less attention is whether the model is identifiable in terms of the causal ordering  $\mathbf{P}$ . In fact, it is not in general: specifically, there may exist many permutation matrices  $\mathbf{P}$  and strictly lower triangular matrices  $\mathbf{T}$  such that the generated data has the same distribution and the generating permutation cannot be identified. For instance, in the degenerate case  $\mathbf{B} = \mathbf{T} = \mathbf{0}$ , any permutation matrix  $\mathbf{P}$  is equally valid and gives the same data distribution. As is well-known, a DAG in general defines only a partial order in the sense that for some pairs of variables, we cannot necessarily say which is “earlier” and which is “later”. Thus, to make the causal ordering well-defined, we need further assumptions, as will be considered below.<sup>1</sup>

**Multi-view ICA** A multi-view version of ICA is of great practical interest. One might obtain a number of views of the same data that might be, for example, different subjects in a biomedical context, different users in more technological applications, or different measurement systems of the same physical phenomenon. A multi-view extension of ICA can then be defined in various ways. Here, we consider the case where the components are, at least partly, shared over views, while the mixing matrices (as well as optional noise terms) are view-dependent.

This leads to the definition of Shared ICA [20, 1]:

$$\mathbf{x}^i = \mathbf{A}^i(\mathbf{s} + \mathbf{n}^i) \quad (4)$$

where  $\mathbf{x}^i$  are the different views indexed by the view index  $i$ . Recently, identifiability conditions have been explored for such multi-view ICA models. On the one hand, it is obvious that if the components are non-Gaussian, the Shared ICA model reduces to a standard ICA model when stacking the different views in a single vector, and hence identifiable. But Richard et al. [20], Anderson et al. [1] showed the surprising result that even if more than one component is Gaussian, the model can still be identifiable if the variances of the noises  $\mathbf{n}^i$  are sufficiently diverse.

### 3 A Linear Multi-View Acyclic Model

Next, we propose a new multi-view model for causal discovery. It is a generalization of LiNGAM, but we generalize its identifiability to the Gaussian case.

**Definition of a multi-view model for causal discovery** We can extend the model in Eq. 2 to the setup where the observations are collected from different views  $i \in \llbracket 1, m \rrbracket$ . In such a multi-view context, one can impose different conditions to exploit the group structure: for example, the causal order  $\mathbf{P}$  could be common over the views, or there might be some similarities between the disturbances.

We choose to model the disturbances as a sum of *common disturbances*  $\mathbf{s}$  and *view-specific noises*  $\mathbf{n}^i$ , inspired by multi-view ICA in Eq. 4. We thus define a generalization of the model in Eq. 2 as

$$\mathbf{x}^i = \mathbf{B}^i \mathbf{x}^i + \mathbf{s} + \mathbf{n}^i \quad (5)$$

where each  $\mathbf{B}^i$  is a DAG, and we make the following statistical assumptions: 1) The common disturbances  $s_j$  (i.e. the entries of  $\mathbf{s}$ ) are all mutually independent, but no assumption is made on their marginal distributions, such as their non-Gaussianity. 2) The view-specific noises  $n_j^i$  are assumed to depend on the view  $i$ , in the sense of satisfying  $\mathbf{n}^i \sim \mathcal{N}(\mathbf{0}, \mathbf{\Sigma}^i)$ , where the  $\mathbf{\Sigma}^i$  are diagonal matrices. 3) The vectors  $\mathbf{s}$  and  $\mathbf{n}^i, i = 1 \dots, m$  are assumed mutually independent.

**Two scenarios for causal ordering** We consider two different scenarios for the  $\mathbf{B}^i$ . On the one hand, we can assume that the  $\mathbf{B}^i$  are independent of each other. That means that each  $\mathbf{B}^i$  can be decomposed with its own causal ordering matrix  $\mathbf{P}^i$  and lower diagonal matrix  $\mathbf{T}^i$  as

$$\mathbf{B}^i = (\mathbf{P}^i)^\top \mathbf{T}^i \mathbf{P}^i . \quad (6)$$

---

<sup>1</sup>One would argue that in some cases,  $\mathbf{P}$  is not even well-defined, and thus it cannot be identifiable, and it is not appropriate to use the concept of identifiability. We prefer here to confound the concepts in the sense that we talk about identifiability of  $\mathbf{P}$  if it is uniquely defined and can be uniquely recovered from the data. A more rigorous justification could be developed by assuming a hierarchical data generation process, where the  $\mathbf{P}$  and  $\mathbf{T}$  are generated first, and the  $\mathbf{B}$  is generated based on them. In that case, if the decomposition of  $\mathbf{B}$  is unique, and  $\mathbf{B}$  is identifiable, also  $\mathbf{P}$  is identifiable in the conventional statistical sense.

This we call the model with *multiple causal orderings*. On the other hand, we consider a constrained case where the causal orders are shared by all views. This means that each  $\mathbf{B}^i$  is decomposed as

$$\mathbf{B}^i = \mathbf{P}^\top \mathbf{T}^i \mathbf{P} \quad (7)$$

where the causal ordering  $\mathbf{P}$  of the DAGs is the same across views. This latter case we call the model with *shared causal ordering*. Such a shared  $\mathbf{P}$  or causal order contains information about all views and can be very useful when estimating view-specific causalities is too inaccurate. If the amount of data per view is very limited, such a shared causal ordering may be the only quantity that can be reliably estimated from the data.

This completes the definition of our Linear Multi-View Acyclic Model (LiMVAM). It has two variants depending on whether the causal orderings are constrained to be shared or not.

**Relation to Multi-view ICA** Our model can be rewritten as a multi-view ICA model as in Eq. 4, just like in the case of LiNGAM. Thus, the methods developed for multi-view ICA can be used to estimate the matrices  $\mathbf{A}^i$ , as well as to analyze its identifiability. Again, it is important to note that the view-dependent mixing matrix  $\mathbf{A}^i$  is structured: it is specifically equal to  $\mathbf{A}^i = (\mathbf{I} - \mathbf{B}^i)^{-1}$ ; in the shared causal ordering case, even further structure is imposed. Importantly, the theory of Shared ICA *does not require the common disturbances  $\mathbf{s}$  to be non-Gaussian* [20, 1], as soon as there are at least 3 views and there is sufficient diversity in the view-specific noises; this condition will be made rigorous in the next section. This makes our multi-view model more widely applicable as well: we can prove its identifiability regardless of the Gaussianity of the common disturbances  $\mathbf{s}$ .

## 4 Identifiability theory

Now we proceed to show the identifiability of the proposed model, in its different variants. As in Richard et al. [20], the following assumption is central.

**Assumption 1** (Noise diversity) *Let  $j$  and  $j'$ ,  $j \neq j'$ , be the indices of two Gaussian common disturbances in  $\mathbf{s}$ . Then, the sequences  $(\Sigma_{jj}^i)_{i=1,\dots,m}$  and  $(\Sigma_{j'j'}^i)_{i=1,\dots,m}$  are different.*

The following theorem gives a fundamental identifiability result, ensuring the identifiability of the causal matrices  $\mathbf{B}^i$  under Assumption 1.

**Theorem 2** (Identifiability of the causal matrices) *Under Assumption 1, the LiMVAM model (whether with multiple or shared causal orderings) is identifiable in the sense that the parameters  $\mathbf{B}^i$  and  $\Sigma^i$  are identifiable.*

We reiterate that no assumption of non-Gaussianity is made here, only that shared Gaussian disturbances have enough noise diversity according to Assumption 1.

Next, we proceed to the question of the identifiability of the causal ordering. As mentioned above, the identifiability of the  $\mathbf{B}^i$  does not necessarily mean that their decomposition in Eq. 7 with  $\mathbf{T}^i$  and  $\mathbf{P}$  (or in Eq. 6 with  $\mathbf{T}^i$  and  $\mathbf{P}^i$ ) is unique. Here, with possible abuse of terminology, we say that the  $\mathbf{P}$  is “identifiable” if it can be uniquely defined based on the  $\mathbf{B}^i$  (see footnote 1 above for a discussion on this point), and we thus consider  $\mathbf{P}$  as if it were a parameter of the model.

It turns out that in the view-specific  $\mathbf{P}^i$  case, identifiability is obtained by assuming that the directed acyclic graph  $\mathbf{B}^i$  is dense enough in each view, as formalized in the following assumption. However, since the  $\mathbf{B}^i$  can be permuted to strictly lower triangular matrices, they cannot have more than  $\frac{p(p-1)}{2}$  non-zero entries.

**Assumption 2** (Dense connectivity in each view) *For each view  $i$ , the matrix  $\mathbf{B}^i$  has exactly  $\frac{p(p-1)}{2}$  non-zero entries.*

Using Assumption 2, the following theorem states that, in addition to identifying  $\mathbf{B}^i$  and  $\Sigma^i$ , one can also identify  $\mathbf{T}^i$  and  $\mathbf{P}^i$ .

**Theorem 3** (Identifiability of multiple causal orderings) *Consider the LiMVAM model with multiple causal orderings. Consider the quantities  $(\Sigma^1, \dots, \Sigma^m, \mathbf{P}^1, \dots, \mathbf{P}^m, \mathbf{T}^1, \dots, \mathbf{T}^m)$  as the set of parameters to be estimated. Under Assumptions 1 and 2, all these parameters are identifiable.*

However, Assumption 2 may be considered rather severe because it prevents the strictly lower triangular part of  $\mathbf{T}^i$  matrices from being sparse. Moreover, in the case of view-specific orderings  $\mathbf{P}^i$ , the main quantity of interest is probably  $\mathbf{B}^i$  rather than  $\mathbf{T}^i$  and  $\mathbf{P}^i$ , which limits the interest of Theorem 3.

On the other hand, the scenario of a shared  $\mathbf{P}$  is very interesting and specific to the multi-view model. In fact, the identifiability in this scenario can be obtained with weaker conditions. Consider the following assumption.

**Assumption 3** (Dense connectivity when pooled across views) *There exists a permutation  $\bar{\mathbf{P}}$  such that the matrices  $\bar{\mathbf{T}}^i = \bar{\mathbf{P}}\mathbf{B}^i\bar{\mathbf{P}}^\top$  are strictly lower triangular, and for each entry  $(j, k)$  with  $j > k$ , there is at least one view  $i$  such that  $\bar{\mathbf{T}}_{j,k}^i \neq 0$ .*

Under the DAG constraint with shared causal ordering, Assumption 2 implies Assumption 3. So, Assumption 3 is much weaker than Assumption 2, as it allows the  $\mathbf{T}^i$  to be very sparse. This is especially the case when the number of views is large, since only one non-zero entry is required over all views. The following theorem states the identifiability of our model in the case of a shared  $\mathbf{P}$  and under Assumptions 1 and 3.

**Theorem 4** (Identifiability of a shared causal ordering) *Consider the LiMVAM model with shared causal ordering. Consider the quantities  $(\Sigma^1, \dots, \Sigma^m, \mathbf{P}, \mathbf{T}^1, \dots, \mathbf{T}^m)$  as the set of parameters to be estimated. Under Assumptions 1 and 3, all these parameters are identifiable.*

In other words, the *common* causal ordering  $\mathbf{P}$  is now perfectly identifiable, and under weaker conditions than above. We point out that this last part of our identifiability theory is based on a very novel approach specific to the multi-view case. The proofs of the theorems are given in Appendix A.

## 5 Estimation of the model

Next, we propose an estimation algorithm for our new model. It is essentially a combination of the ICA-based estimation procedure by Shimizu et al. [26], combined with the Shared ICA methods by Richard et al. [20]. Thus, we call it Multi-view ICA-based Causal Discovery (MICaDo).

The method consists of two steps: first, find the causal matrices  $\mathbf{B}^i$  by means of Shared ICA, then find their DAG decomposition into  $\mathbf{T}^i$  and  $\mathbf{P}^i$ . The procedure is summarized in Algorithm 1. Next, we describe the method in more detail.

**Finding the causal matrices** In general, an ICA algorithm yields  $\mathbf{W}^i$  which is the inverse of the true underlying  $\mathbf{A}^i = (\mathbf{I} - \mathbf{B}^i)^{-1}$ , up to an unknown scale-permutation matrix  $\mathbf{M}$

$$(\mathbf{A}^i)^{-1} = \mathbf{M}\mathbf{W}^i . \quad (8)$$

To determine  $\mathbf{M}$ , we use the structure of the underlying  $(\mathbf{A}^i)^{-1} = (\mathbf{I} - \mathbf{B}^i)$ : it has diagonal of ones. As a first approach, we could determine  $\mathbf{M}$  by solving

$$\min_{\mathbf{K}} \sum_{j=1}^p ((\mathbf{K}\mathbf{W}^i)_{jj} - 1)^2 \quad (9)$$

over scale-permutation matrices, and separately for each view. However, we know from the theory of Shared ICA [20] that the unknown permutation matrix is the same for all views. Thus, we can adapt the simple two-step approach by Shimizu et al. [26]. We propose to compute, rather heuristically:

1. Find a permutation matrix  $\mathbf{K}$  such that  $\mathbf{K}\mathbf{W}$  has a non-zero diagonal, by solving:

$$\min_{\mathbf{K}} \sum_{j=1}^p \frac{1}{|(\mathbf{K}\mathbf{W})_{jj}|} , \quad \mathbf{W} = \sum_{i=1}^m \text{abs}(\mathbf{W}^i) , \quad (10)$$

where the abs operator takes the absolute value of each entry.

2. Rescale the rows of  $\mathbf{K}$  to ensure that  $\mathbf{K}\mathbf{W}$  has a diagonal of ones. Specifically, update for all  $j, k$ :

$$\mathbf{K}_{jk} \leftarrow \frac{\mathbf{K}_{jk}}{(\mathbf{K}\mathbf{W})_{jj}} . \quad (11)$$

Now that  $\mathbf{M}$  is determined, we know the true  $\mathbf{A}^i$  and use the identity  $\mathbf{B}^i = \mathbf{I} - (\mathbf{A}^i)^{-1}$  to obtain the causal matrix  $\mathbf{B}^i$ .

**Find the DAG decompositions** In the case of multiple causal orderings, once each  $\mathbf{B}^i$  is obtained, we find its DAG decomposition using the structure of

$$\mathbf{T}^i = \mathbf{P}^i \mathbf{B}^i (\mathbf{P}^i)^\top \quad (12)$$

which is strictly lower triangular. Hence we can jointly obtain  $\mathbf{T}^i$  and  $\mathbf{P}^i$  by solving

$$\min_{\mathbf{K}^i} \sum_{l \geq k} (\mathbf{K}^i \mathbf{B}^i (\mathbf{K}^i)^\top)_{kl}^2 . \quad (13)$$

The minimizer is the permutation matrix  $\mathbf{P}^i$ , and at the minimum, the matrix from which we take squared elements is  $\mathbf{T}^i$ . On the other hand, if the causal orderings are shared across views, we instead solve

$$\min_{\mathbf{K}} \sum_{l \geq k} (\mathbf{K} \mathbf{B} \mathbf{K}^\top)_{kl}^2 , \quad \mathbf{B} = \sum_{i=1}^m \text{abs}(\mathbf{B}^i) . \quad (14)$$

---

**Algorithm 1** MICaDo

---

1. Determine the unmixing matrices  $\mathbf{W}^i$ , by running the Shared ICA estimation algorithm on the data.
2. Determine the permutation indeterminacy  $\mathbf{M}$ . To do this, first solve

$$\min_{\mathbf{M}} \sum_{j=1}^p \frac{1}{|(\mathbf{M}\mathbf{W})_{jj}|} , \quad \mathbf{W} = \sum_{i=1}^m \text{abs}(\mathbf{W}^i) , \quad (15)$$

and then update

$$\mathbf{M}_{ij} \leftarrow \frac{\mathbf{M}_{ij}}{(\mathbf{M}\mathbf{W})_{ii}} . \quad (16)$$

3. Determine the causal matrices  $\mathbf{B}^i = \mathbf{I} - \mathbf{M}\mathbf{W}^i$ .
4. Determine the causal ordering. If the causal ordering  $\mathbf{P}^i$  is view-dependent, solve

$$\min_{\mathbf{P}^i} \sum_{l \geq k} (\mathbf{P}^i \mathbf{B}^i (\mathbf{P}^i)^\top)_{kl}^2 . \quad (17)$$

If the causal ordering  $\mathbf{P}$  is shared across views, solve instead

$$\min_{\mathbf{P}} \sum_{l \geq k} (\mathbf{P} \mathbf{B} \mathbf{P}^\top)_{kl}^2 , \quad \mathbf{B} = \sum_{i=1}^m \text{abs}(\mathbf{B}^i) . \quad (18)$$


---

Note that in the special case when there is only a single view and at most one Gaussian disturbance, our estimation algorithm for MICaDo recovers the ICA-based estimation for LiNGAM proposed by Shimizu et al. [26].

## 6 Experiments

Our Python code for the following experiments is available at the following link <https://github.com/AmbroiseHeurtebise/MICaDo>. It is heavily based on the Python library for causal discovery <https://github.com/cdt15/lingam>.

### 6.1 Simulations

In the following synthetic experiment, data are generated according to the LiMVAM model Eq. 5 with  $m = 5$  views,  $p = 4$  variables, and a shared causal ordering  $\mathbf{P}$ . The case with view-specific orderings  $\mathbf{P}^i$



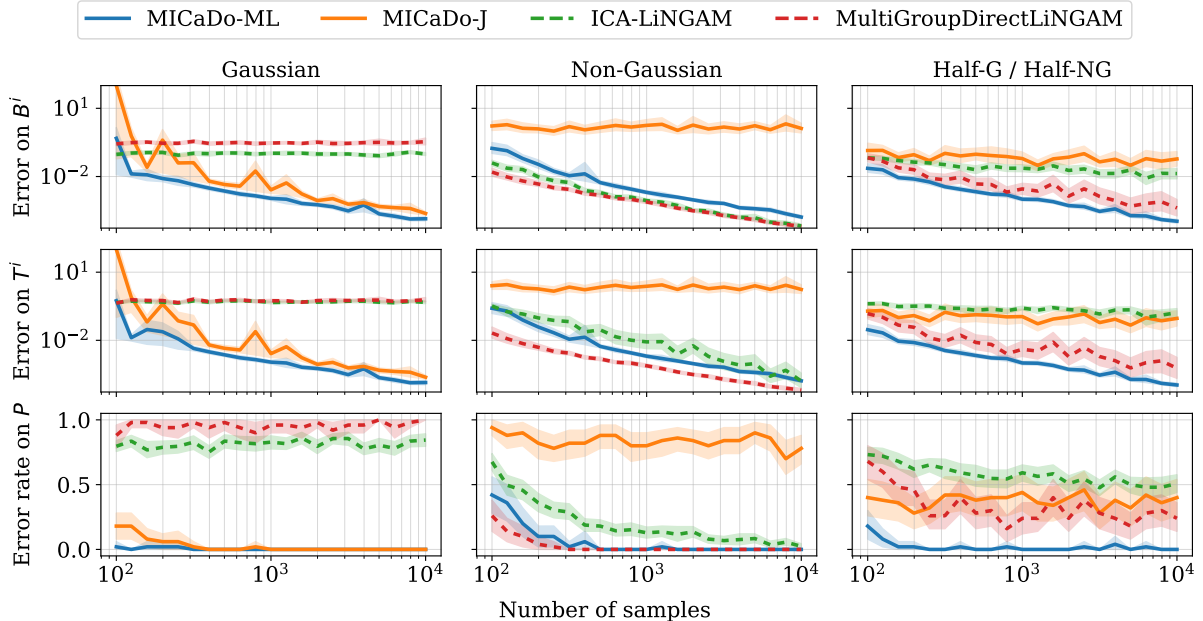


Figure 1: Separation performance of ICA-LiNGAM [26], MultiGroupDirectLiNGAM [24] and two versions of our MICaDo method (depending on which version of ShICA is chosen) in the *shared causal ordering* context and while varying the number of samples. Left column: all disturbances are Gaussian. Middle column: all disturbances are non-Gaussian and the noise variances are equal. Right column: half of the disturbances are Gaussian and the other half are non-Gaussian. There are three different metrics: the  $\ell_2$ -distance between true and estimated causal effect matrices  $\mathbf{B}^i$  (upper row), the  $\ell_2$ -distance between true and estimated matrices  $\mathbf{T}^i$  (middle row), and the rate of failed estimated causal orderings  $\mathbf{P}$  over all repetitions (lower row; lower is better). We used 50 different seeds.

is explored in Appendix B.1. The disturbances in  $\mathbf{s}$  can be either Gaussian or non-Gaussian: Gaussian disturbances  $s_j$  are generated from a standardized Gaussian and their corresponding noises  $n_j^i$  have standard deviation  $\Sigma_{jj}^i$ , obtained by sampling from a uniform density between 0 and 1, while non-Gaussian disturbances are generated from a Laplace distribution (with scale parameter equal to  $\frac{1}{2}$ ) and their corresponding noises all have a standard deviation of  $\frac{1}{2}$ . The practical generation proceeds by the equivalent Shared ICA model in Eq. 4, where the mixing matrices are generated according to  $\mathbf{A}^i = \mathbf{P}^\top (\mathbf{I} - \mathbf{T}^i)^{-1} \mathbf{P}$ , where  $\mathbf{P}$  is a randomly chosen permutation matrix and  $\mathbf{T}^i$  are strictly lower triangular matrices whose non-zero entries are standardized Gaussian.

As in Richard et al. [20], we study three cases where either all disturbances are Gaussian, all disturbances are non-Gaussian, or half of the disturbances are Gaussian and the other half are non-Gaussian. We vary the number of samples  $n$  between  $10^2$  and  $10^4$  and display in Fig. 1 the  $\ell_2$  distance between true and estimated causal effect matrices  $\mathbf{B}^i$ , the  $\ell_2$  distance between true and estimated matrices  $\mathbf{T}^i$ , and the rate of unsuccessfully estimated causal orders  $\mathbf{P}$ . Specifically, for each run, the measure of error in estimating  $\mathbf{P}$  is 1 if the permutation was not recovered and 0 otherwise.

We plot two different versions of our method. First, MICaDo-ML, which relies on ShICA-ML, a likelihood-based method that can handle both Gaussian and non-Gaussian disturbances (sources). Second, MICaDo-J, which relies on ShICA-J, a method based on joint-diagonalization of covariances, which does not use non-Gaussianity but is faster. These we compare to MultiGroupDirectLiNGAM [24] and ICA-LiNGAM [26]. Given that ICA-LiNGAM is a single-view algorithm, we apply it separately to each view. The experiment is repeated 50 times using different seeds.

We can see in Figure 1 that MICaDo-ML achieves the best results (just ahead of MICaDo-J) when disturbances are Gaussian and the sample size is just above 100. The performance gap increases with the sample size, as MultiGroupDirectLiNGAM and ICA-LiNGAM completely fail to recover the parameters to the point where they do not even seem to depend on the number of samples. This was expected as these methods are not designed to deal with Gaussian sources. On the other hand, in the classical context of non-Gaussian disturbances, MultiGroupDirectLiNGAM seems to produce slightly better results than MICaDo-ML, but the results of the two methods remain close. ICA-LiNGAM achieves a low error in the estimation of the matrices  $\mathbf{B}^i$ , but, as a single-view algorithm, it is not designed to look for a shared

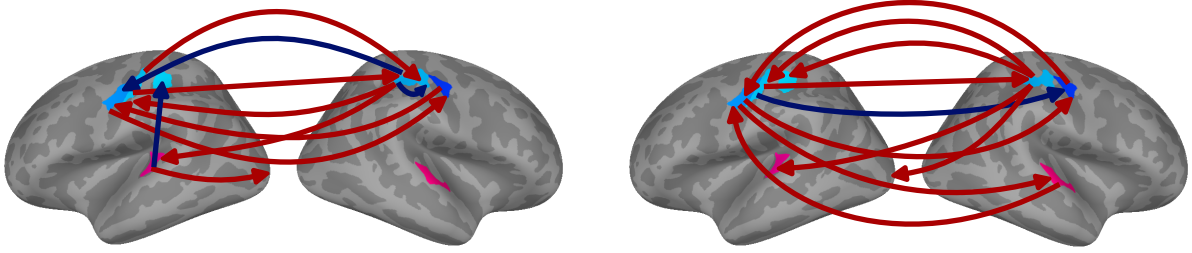


Figure 2: Top ten most important causal effects on two different runs. Each run was performed on the data of 49 randomly chosen subjects. We took the median of the causal effect matrices and picked the 10 highest entries in absolute value. Red arrows represent positive effects and blue arrows negative effects.

matrix  $\mathbf{P}$ , which causes the drop in performance in the second and third rows. In turn, MICaDo-J fails to estimate the parameters because it is designed to search for noise diversity, making this context its adversarial case. Finally, when half of the disturbances are Gaussian and the other half are non-Gaussian, MICaDo-ML outperforms the other methods. MultiGroupDirectLiNGAM is close behind in terms of estimating  $\mathbf{B}^i$  and  $\mathbf{T}^i$  but has more difficulty with the estimation of the ordering  $\mathbf{P}$ . In addition, MICaDo-J (and ICA-LiNGAM respectively) perform better than in the pure Gaussian (and pure non-Gaussian) case, but they struggle to improve performance as the sample size increases.

Overall, MICaDo-ML is the only one of the four methods that produces good results in all scenarios, making it a safe choice when no information on the Gaussianity of the disturbances is available. Further experiments are conducted in Appendix B.1.

## 6.2 Real brain imaging data

Next, we performed experiments on magnetoencephalography (MEG) data measuring human brain activity. MEG data has a high temporal resolution, so typically methods related to Granger causality are used. However, we are here interested in analyzing the *envelopes*, *energies*, or *powers* (these three terms meaning essentially the same thing) of *oscillatory* signals. Such energies are correlates of brain activity that are not captured in the raw amplitudes of the signals. The energies also change very slowly (on the time-scale of one second), while the underlying brain activity being measured is likely to change much more quickly. Thus, it is appropriate to use a model of instantaneous causality, as in a SEM or our model, to analyze causal connections between the energies (or rather, the brain activity that they reflect).

### 6.2.1 Data and preprocessing

We used the Cam-CAN dataset, which is the largest publicly available MEG dataset [23, 31]. We considered the "sensorimotor task" during which each participant had to respond with a right index finger button press to auditory/visual stimuli. The auditory stimuli were binaural pure tones. The visual stimuli were checkerboards presented both to the left and right of a central fixation for 34-ms duration. Given the nature of the stimuli and the active task, the neural activity involves multiple brain regions spread over the cortex (visual, auditory, and motor areas). Also, this task leads to strong signal power modulations during the motor preparation and motor execution. This makes it relevant to the approach at hand.

The original MEG data were acquired with 306 sensors, recorded at 1000 Hz, and band-pass filtered between 0.03 and 330 Hz. All MEG processing was done using the MNE-Python library [7, 8] and we largely followed the pre-processing steps used in Power et al. [19]. We applied a Maxwell filter [30] to improve data quality and a band-pass filter between 8 and 27 Hz to focus on power effects spread over the alpha and beta bands of the brain. This range of waves is supposed to be particularly active in sensorimotor tasks, especially during movement preparation and execution, and it typically shows a characteristic suppression (event-related desynchronization) during movement, followed by a rebound (event-related synchronization) after movement cessation, which is thought to reflect sensorimotor processing and inhibitory mechanisms. In particular, the suppression and rebound are reflected in the energies of the signals, not raw signals.

The data was then parsed into trials synchronized to each button press, with a duration of 4.5 s, including a 1.5 s pre-movement interval. The 4.5 s window length was selected to ensure a sufficient post-movement interval to capture the entire beta rebound response. Trials were excluded if the button press



occurred more than 1 s after the audiovisual cue (indicating poor task performance) or if another button press occurred within the time window. Then, a baseline correction was applied using the pre-movement interval ( $-1.5\text{ s}, -1\text{ s}$ ). The procedure led to about 60 trials per participant on average.

Next, we performed a cortical projection. First, each participant’s MRI (additionally given in the Cam-CAN database) was segmented using FreeSurfer [5]. The segmentation provided a digitization of the cortical surface for source estimation, a transformation to the average brain (i.e. fsaverage) for spatial normalization and group statistics, and a boundary element model of the head to provide more accurate calculation of the forward solution. The inverse solution, based on the MNE method [9], allowed to consider cortical region activations for further analysis.

We used the cortical parcellation from [13] to divide the cortical mantle (both hemispheres) into 448 distinct regions and summarized each region by an averaged time course. Then, we selected 10 of the 448 regions based on their known importance in sensorimotor tasks. Specifically, we picked for each hemisphere three regions in the motor cortex (two parcels in the “postcentral” and one in the “precentral”; visible in blue in Fig. 2), one region in the auditory cortex (“superiortemporal” parcel; highlighted in pink), and one region in the visual cortex (“pericalcarine” parcel; not visible in the figure). Note again that the task for the participant is active as right index button presses are triggered by audiovisual stimulations.

For each participant, we thus extracted one time series for each of the 10 regions and fixed the number of trials to 40. Participants with less than 40 trials were discarded and extra trials were averaged. Participants for whom some of the parcels did not have any vertex in the source space were also discarded, resulting in a total of 98 available participants. We performed a Z-score normalization of the time series to correct the depth bias and, importantly, computed the Hilbert *envelope* of the signals to study modulations in cortical source power. Finally, the signals were centered and downsampled from 1000 Hz to 10 Hz due to the slowly changing nature of the envelopes (energies). The final dataset consisted of 98 subjects, 10 brain regions, and 1760 time points.

### 6.2.2 Causal analysis methods and results

We applied MICaDo-ML to these data to recover the causal effect matrices  $\mathbf{B}^i$  and  $\mathbf{T}^i$  and the shared permutation  $\mathbf{P}$ . Although not assumed in the model, one can assume that the causal effects present some similarities among views. For example, causal effects from one brain region to another might be comparable from one participant to another. So, we computed the element-wise median of the  $\mathbf{B}^i$  matrices to study shared effects. Fig. 2 shows the top ten highest causal effects in absolute value for two repetitions of this experiment with 49 randomly chosen subjects each. Red arrows represent positive effects and blue arrows negative effects.

We can see in the figure that many arrows point from one hemisphere to the corresponding region in the other hemisphere (especially in the primary motor cortex and the primary somatosensory cortex) which confirms the fact that symmetric regions are highly correlated [14]. We can also see that many arrows point to or from the postcentral regions of the brain, in particular the “postcentral-8” parcel which is thought to be deeply involved in motor processing tasks involving the hand [3]. Four more brain plots are displayed in Appendix B.1 and confirm these observations.

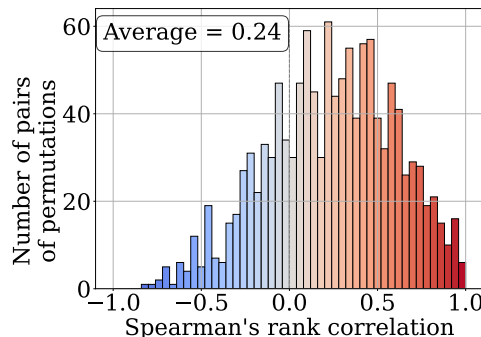


Figure 3: Histogram of the Spearman’s rank correlations between permutation matrices  $\mathbf{P}$ . Each of the 50 runs was performed on the data of 50% randomly chosen participants and outputted a matrix  $\mathbf{P}$ , resulting in a total of 1225 correlations.

To evaluate the consistency of the results, we performed 50 runs of the same experiment. In each run, we randomly drew 50% of the participants and used MICaDo-ML to recover the parameters. We

focused here on measuring the consistency of the common causal ordering, which is a quantity specific to our multi-view framework. To measure the correlation between the estimated permutations  $\mathbf{P}$ , we used Spearman’s rank correlation on the orderings. The obtained correlation matrix is displayed in Appendix B and the 1225 correlations are given in the histogram in Fig. 3. We can see that the obtained orderings are mainly positively correlated across runs and the average correlation is 0.24. This suggests that the estimated parameters are reasonably consistent across runs.

## 7 Discussion

### 7.1 Related work

While the Introduction 1 already discussed related work, we discuss next the connection to Shimizu [24] in more detail. The fundamental difference is that we assume the disturbances have some shared information across views and can be Gaussian, whereas Shimizu [24] estimates disturbances that are view-dependent and necessarily non-Gaussian. Unlike Shimizu [24], we prove identifiability results requiring only Gaussianity. Moreover, the estimation methods are different: Shimizu [24] use an extension of DirectLiNGAM [27] to multiple views, while we combine methods from Shared ICA Richard et al. [20] and the original ICA-based LiNGAM [26].

A related very general framework, allowing for various kinds of interventions, was proposed by Mooij et al. [16]. On the other hand, a related “multi-context” approach, where the disturbances are not necessarily related at all while the DAGs are, was proposed by Sturma et al. [29].

### 7.2 Future work

Typically, optimizing over permutations has a worst-case complexity that is cubic in the number of variables,  $O(p^3)$ , but that plagues much of LiNGAM literature. We leave the design of more computationally efficient algorithms for future work. Likewise, methods such as DirectLiNGAM [27] or PairwiseLiNGAM [12] might be useful and adaptable to the multi-view context.

One variant of the model that might be useful in a very low-data regime is the one in which the  $\mathbf{B}^i$  are the same over  $i$ . This should be almost trivial to implement on the algorithmic level, while the identifiability is already implied by our results under the same assumptions.

## 8 Conclusion

We propose a new model for causal discovery in the multi-view linear-DAG case. Surprisingly, we show that the model is fully identifiable even with Gaussian disturbances. The only thing that is needed is that the variances of the disturbances have some weak variability over the views. The results rely on a little-known framework for multi-view ICA [20, 1]. We develop algorithms that either use the covariance structure only, or automatically use both non-Gaussianity or the Gaussian covariance structure. Results on brain imaging data are promising.

**Acknowledgements** Ambroise Heurtebise is supported by grant ANR-20-CHIA-0016 granted to Alexandre Gramfort while at Inria. Omar Chehab is supported by funding from the French ANR JCJC WOS granted to Anna Korba. Aapo Hyvärinen was supported by a Fellowship from CIFAR.

## References

- [1] Anderson, M., Fu, G., Phlypo, R., and Adali, T. (2013). Independent vector analysis: Identification conditions and performance bounds. *IEEE Transactions on Signal Processing*, 62:4399–4410.
- [2] Bollen, K. A. (1989). *Structural equations with latent variables*, volume 210. John Wiley & Sons.
- [3] Braun, C., Haug, M., Wiech, K., Birbaumer, N., Elbert, T., and Roberts, L. E. (2002). Functional organization of primary somatosensory cortex depends on the focus of attention. *Neuroimage*, 17(3):1451–1458.
- [4] Comon, P. (1994). Independent component analysis, a new concept? *Signal Processing*, 36(3):287–314. Higher Order Statistics.

- [5] Dale, A. M., Fischl, B., and Sereno, M. I. (1999). Cortical surface-based analysis: I. segmentation and surface reconstruction. *Neuroimage*, 9(2):179–194.
- [6] Genin, K. (2021). Statistical undecidability in linear, non-gaussian causal models in the presence of latent confounders. In Ranzato, M., Beygelzimer, A., Dauphin, Y., Liang, P., and Vaughan, J. W., editors, *Advances in Neural Information Processing Systems*, volume 34, pages 13564–13574. Curran Associates, Inc.
- [7] Gramfort, A., Luessi, M., Larson, E., Engemann, D. A., Strohmeier, D., Brodbeck, C., Goj, R., Jas, M., Brooks, T., Parkkonen, L., and Hämäläinen, M. (2013). Meg and eeg data analysis with mne-python. *Frontiers in Neuroscience*, 7.
- [8] Gramfort, A., Luessi, M., Larson, E., Engemann, D. A., Strohmeier, D., Brodbeck, C., Parkkonen, L., and Hämäläinen, M. S. (2014). Mne software for processing meg and eeg data. *NeuroImage*, 86:446–460.
- [9] Hämäläinen, M. S. and Ilmoniemi, R. J. (1994). Interpreting magnetic fields of the brain: minimum norm estimates. *Medical & Biological Engineering & Computing*, 32(1):35–42.
- [10] Hoyer, P., Janzing, D., Mooij, J. M., Peters, J., and Schölkopf, B. (2008). Nonlinear causal discovery with additive noise models. *Advances in neural information processing systems*, 21.
- [11] Hyvärinen, A., Karhunen, J., and Oja, E. (2001). *Independent Component Analysis*. Wiley Inter-science.
- [12] Hyvärinen, A. and Smith, S. M. (2013). Pairwise likelihood ratios for estimation of non-Gaussian structural equation models. *J. of Machine Learning Research*, 14:111–152.
- [13] Khan, S., Hashmi, J. A., Mamashli, F., Michmizos, K., Kitzbichler, M. G., Bharadwaj, H., Bekhti, Y., Ganesan, S., Garel, K.-L. A., Whitfield-Gabrieli, S., Gollub, R. L., Kong, J., Vaina, L. M., Rana, K. D., Stufflebeam, S. M., Hämäläinen, M. S., and Kenet, T. (2018). Maturation trajectories of cortical resting-state networks depend on the mediating frequency band. *NeuroImage*, 174:57–68.
- [14] Li, A., Yetkin, F. Z., Cox, R., and Houghton, V. M. (1996). Ipsilateral hemisphere activation during motor and sensory tasks. *American Journal of Neuroradiology*, 17(4):651–655.
- [15] Monti, R. P., Zhang, K., and Hyvärinen, A. (2019). Causal discovery with general non-linear relationships using non-linear ICA. In *Proc. 35th Conf. on Uncertainty in Artificial Intelligence (UAI2019)*, Tel Aviv, Israel.
- [16] Mooij, J. M., Magliacane, S., and Claassen, T. (2020). Joint causal inference from multiple contexts. *Journal of machine learning research*, 21(99):1–108.
- [17] Peters, J. and Bühlmann, P. (2014). Identifiability of gaussian structural equation models with equal error variances. *Biometrika*, 101(1):219–228.
- [18] Peters, J., Janzing, D., and Schölkopf, B. (2017). *Elements of causal inference: foundations and learning algorithms*. The MIT Press.
- [19] Power, L., Allain, C., Moreau, T., Gramfort, A., and Bardouille, T. (2023). Using convolutional dictionary learning to detect task-related neuromagnetic transients and ageing trends in a large open-access dataset. *NeuroImage*, 267:119809.
- [20] Richard, H., Ablin, P., Thirion, B., Gramfort, A., and Hyvarinen, A. (2021). Shared independent component analysis for multi-subject neuroimaging. In *Advances in Neural Information Processing Systems*, volume 34, pages 29962–29971. Curran Associates, Inc.
- [21] Richard, H., Gresele, L., Hyvarinen, A., Thirion, B., Gramfort, A., and Ablin, P. (2020). Modeling shared responses in neuroimaging studies through multiview ica. *Advances in Neural Information Processing Systems*, 33:19149–19162.
- [22] Richardson, T. and Spirtes, P. (2002). Ancestral graph Markov models. *The Annals of Statistics*, 30(4):962 – 1030.

- [23] Shafto, M. A., Tyler, L. K., Dixon, M., Taylor, J. R., Rowe, J. B., Cusack, R., Calder, A. J., Marslen-Wilson, W. D., Duncan, J. S., Dalgleish, T., Henson, R. N. A., Brayne, C., and Matthews, F. E. (2014). The cambridge centre for ageing and neuroscience (cam-can) study protocol: a cross-sectional, lifespan, multidisciplinary examination of healthy cognitive ageing. *BMC Neurology*, 14.
- [24] Shimizu, S. (2012). Joint estimation of linear non-gaussian acyclic models. *Neurocomputing*, 81:104–107.
- [25] Shimizu, S. (2022). *Statistical Causal Discovery: LiNGAM Approach*. Springer.
- [26] Shimizu, S., Hoyer, P. O., Hyvärinen, A., Kerminen, A., and Jordan, M. (2006). A linear non-gaussian acyclic model for causal discovery. *Journal of Machine Learning Research*, 7(10).
- [27] Shimizu, S., Inazumi, T., Sogawa, Y., Hyvarinen, A., Kawahara, Y., Washio, T., Hoyer, P. O., Bollen, K., and Hoyer, P. (2011). Directlingam: A direct method for learning a linear non-gaussian structural equation model. *Journal of Machine Learning Research-JMLR*, 12(Apr):1225–1248.
- [28] Spirtes, P., Glymour, C., and Scheines, R. (2001). *Causation, prediction, and search*. MIT press, second edition edition.
- [29] Sturma, N., Squires, C., Drton, M., and Uhler, C. (2023). Unpaired multi-domain causal representation learning. In Oh, A., Naumann, T., Globerson, A., Saenko, K., Hardt, M., and Levine, S., editors, *Advances in Neural Information Processing Systems*, volume 36, pages 34465–34492. Curran Associates, Inc.
- [30] Taulu, S. and Simola, J. (2006). Spatiotemporal signal space separation method for rejecting nearby interference in meg measurements. *Physics in Medicine & Biology*, 51(7):1759.
- [31] Taylor, J. R., Williams, N., Cusack, R., Auer, T., Shafto, M. A., Dixon, M., Tyler, L. K., Cam-CAN, and Henson, R. N. (2017). The cambridge centre for ageing and neuroscience (cam-can) data repository: Structural and functional mri, meg, and cognitive data from a cross-sectional adult lifespan sample. *NeuroImage*, 144:262–269. Data Sharing Part II.
- [32] Zhang, K. and Hyvärinen, A. (2009). On the identifiability of the post-nonlinear causal model. In *Proc. 25th Conference on Uncertainty in Artificial Intelligence (UAI2009)*, pages 647–655, Montréal, Canada.

# Appendix

The paper and appendix are organized as follows.

<b>1</b>	<b>Introduction</b>	<b>1</b>
<b>2</b>	<b>Background</b>	<b>2</b>
<b>3</b>	<b>A Linear Multi-View Acyclic Model</b>	<b>3</b>
<b>4</b>	<b>Identifiability theory</b>	<b>4</b>
<b>5</b>	<b>Estimation of the model</b>	<b>5</b>
<b>6</b>	<b>Experiments</b>	<b>6</b>
6.1	Simulations . . . . .	6
6.2	Real brain imaging data . . . . .	8
6.2.1	Data and preprocessing . . . . .	8
6.2.2	Causal analysis methods and results . . . . .	9
<b>7</b>	<b>Discussion</b>	<b>10</b>
7.1	Related work . . . . .	10
7.2	Future work . . . . .	10
<b>8</b>	<b>Conclusion</b>	<b>10</b>
<b>A</b>	<b>Proofs of Theorems</b>	<b>14</b>
A.1	Technical lemmas . . . . .	14
A.2	Proof of Theorem 1 . . . . .	14
A.3	Proof of Theorem 2 . . . . .	15
A.4	Proof of Theorem 3 . . . . .	15
A.5	Proof of Theorem 4 . . . . .	15
A.6	Proofs of technical lemmas . . . . .	17
A.6.1	Proof of Lemma 5 . . . . .	17
A.6.2	Proof of Lemma 6 . . . . .	18
<b>B</b>	<b>Additional experiments</b>	<b>19</b>
B.1	Additional simulations . . . . .	19
B.2	Additional experiments on real data . . . . .	20

## A Proofs of Theorems

**Defining a domain connecting ICA and SEM parameters** In the following proofs, we define the set

$$\mathcal{W} = \{\mathbf{W} \in \mathbb{R}^{p \times p} \mid \text{there exist a permutation matrix } \mathbf{P} \text{ and a strictly lower triangular matrix } \mathbf{T} \text{ such that } \mathbf{W} = \mathbf{P}^\top(\mathbf{I} - \mathbf{T})\mathbf{P}\} \quad (19)$$

as the domain of the “unmixing matrices”  $\mathbf{W} = \mathbf{A}^{-1}$  in the ICA model from Eq. 3, that are compatible with the DAG structure in the structural equation model (SEM) from Eq. 2. As noted in the main text, unmixing matrices are not constrained in the ICA model, except by invertibility (and possibly by normalizing their rows). However, in the context of SEM estimation, the requirement that  $\mathbf{W} = \mathbf{I} - \mathbf{B}$  belongs to the set  $\mathcal{W}$  is a key structural constraint. Furthermore, it should be noted that finding  $\mathbf{W}$  is equivalent to finding  $\mathbf{B}$ , since they are related by  $\mathbf{B} = \mathbf{I} - \mathbf{W}$ .

### A.1 Technical lemmas

The following two lemmas are about matrices in the context of DAGs. They are used in the proofs of Theorems 1, 2, 3, and 4, and are proven in Appendix A.6.

The basic identifiability results for the causal matrices  $\mathbf{B}^i$  use the following:

**Lemma 5** *Consider  $\mathbf{W}, \mathbf{W}' \in \mathcal{W}$  defined in Eq. 19,  $\mathbf{K}$  a permutation matrix and  $\mathbf{D}$  a diagonal matrix (of signs and scalings in the ICA context). Then*

$$\mathbf{W}' = \mathbf{DKW} \implies \mathbf{K} = \mathbf{D} = \mathbf{I} . \quad (20)$$

On the other hand, the identifiability results for the causal ordering  $\mathbf{P}$  (or causal orderings  $\mathbf{P}^i$ ) use the following:

**Lemma 6** *Let  $\mathbf{P}$  and  $\mathbf{P}'$  be permutation matrices and  $\mathbf{T}$  and  $\mathbf{T}'$  be strictly lower triangular matrices, such that  $\mathbf{P}^\top \mathbf{T} \mathbf{P} = \mathbf{P}'^\top \mathbf{T}' \mathbf{P}'$ . Assume that  $\mathbf{T}$  contains only non-zero elements in its strictly lower triangular part. Then,  $\mathbf{P} = \mathbf{P}'$  and  $\mathbf{T} = \mathbf{T}'$ .*

### A.2 Proof of Theorem 1

This proof is based on the one from Shimizu et al. [26], which we attempt to make a bit more rigorous. Identifiability was also shown in Shimizu [25, Section 2.3] in the case with 2 components.

Let us transform the SEM

$$\mathbf{x} = \mathbf{B}\mathbf{x} + \mathbf{s} \quad (21)$$

into an ICA model

$$\mathbf{x} = \mathbf{A}\mathbf{s} \quad (22)$$

where the mixing matrix  $\mathbf{A}$  is constrained as  $\mathbf{A}^{-1} = \mathbf{I} - \mathbf{B}$ , and where  $\mathbf{B}$  is a DAG. The assumptions on  $\mathbf{s}$  are identical in SEM and ICA. Given that  $\mathbf{B}$  is a DAG, we have that  $\mathbf{W} = \mathbf{A}^{-1}$  belongs to the set  $\mathcal{W}$  defined in Eq. 19.

Consider two matrices  $\mathbf{W}, \mathbf{W}' \in \mathcal{W}$  that parameterize the same statistical model in Eq. 21 (here, we parameterize by  $\mathbf{W} = \mathbf{I} - \mathbf{B}$  instead of  $\mathbf{B}$ ). Since  $\mathcal{W}$  is included in the space of invertible matrices, we deduce that  $\mathbf{W}$  and  $\mathbf{W}'$  are invertible, which makes them valid unmixing matrices for the same ICA model in Eq. 22. So, from the identifiability theory of ICA [4], we know that there exist a permutation matrix  $\mathbf{K}$  and a sign-scaling matrix  $\mathbf{D}$  (i.e. a diagonal matrix) such that

$$\mathbf{W}' = \mathbf{DKW} . \quad (23)$$

Then, we apply Lemma 5, which shows that being in the domain  $\mathcal{W}$  imposes  $\mathbf{K} = \mathbf{D} = \mathbf{I}$ . Thus, only a single possible solution of the ICA problem is valid, and  $\mathbf{W}$  is fully identifiable (“fully” identifiable is in contrast to conventional ICA theory where some indeterminacies always remain). Since  $\mathbf{B} = \mathbf{I} - \mathbf{W}$ , we deduce that  $\mathbf{B}$  is fully identifiable as well.



### A.3 Proof of Theorem 2

Consider two sets  $\Theta = (\Sigma^1, \dots, \Sigma^m, \mathbf{W}^1, \dots, \mathbf{W}^m)$  and  $\Theta' = (\Sigma'^1, \dots, \Sigma'^m, \mathbf{W}'^1, \dots, \mathbf{W}'^m)$  that parameterize the same statistical model in Eq. 5, with the  $\mathbf{W}^i$  and  $\mathbf{W}'^i$  necessarily belonging to  $\mathcal{W}$ . Note that, as in Appendix A.2, we parameterize by  $\mathbf{W}^i$  instead of  $\mathbf{B}^i$ , but it all boils down to the same thing. First, we use the fact that the domain  $\mathcal{W}$  is included in the space of invertible matrices. Thus, the two sets of  $\mathbf{W}^i$  and  $\mathbf{W}'^i$  matrices are valid sets of unmixing matrices for the same multi-view ICA model in Eq. 4. So, from the identifiability theory of multi-view ICA [20, Theorem 1], we know that there exist a permutation matrix  $\mathbf{K}$  and a sign-scaling matrix  $\mathbf{D}$ , such that for any view  $i \in \llbracket 1, m \rrbracket$ , we have

$$\begin{aligned}\mathbf{W}'^i &= \mathbf{D}\mathbf{K}\mathbf{W}^i \\ \Sigma'^i &= (\mathbf{D}\mathbf{K})\Sigma^i(\mathbf{D}\mathbf{K})^\top.\end{aligned}\tag{24}$$

Then, we apply Lemma 5 (even for one view is enough), which shows that being in the domain  $\mathcal{W}$  imposes  $\mathbf{K} = \mathbf{D} = \mathbf{I}$ .

### A.4 Proof of Theorem 3

In the context of view-specific causal orderings  $\mathbf{P}^i$ , we prove that, under Assumptions 1 and 2, the decomposition of matrices  $\mathbf{B}^i$  into matrices  $\mathbf{T}^i$  and  $\mathbf{P}^i$  is unique.

Consider two sets of parameters  $\Theta = (\Sigma^1, \dots, \Sigma^m, \mathbf{P}^1, \dots, \mathbf{P}^m, \mathbf{T}^1, \dots, \mathbf{T}^m)$  and  $\Theta' = (\Sigma'^1, \dots, \Sigma'^m, \mathbf{P}'^1, \dots, \mathbf{P}'^m, \mathbf{T}'^1, \dots, \mathbf{T}'^m)$  that parameterize the same statistical model in Eq. 5, where  $\mathbf{P}^i, \mathbf{P}'^i$  are permutation matrices, and  $\mathbf{T}^i, \mathbf{T}'^i$  are strictly lower triangular matrices. Note that here we parameterize by  $\mathbf{P}^i$  and  $\mathbf{T}^i$  rather than  $\mathbf{B}^i$  or  $\mathbf{W}^i$ . From Theorem 2, we know that  $\Sigma^i = \Sigma'^i$  and that the resulting causal matrices must be equal:

$$(\mathbf{P}^i)^\top \mathbf{T}^i \mathbf{P}^i = (\mathbf{P}'^i)^\top \mathbf{T}'^i \mathbf{P}'^i.\tag{25}$$

Assumption 2 states that, for each view  $i$ , the matrix  $\mathbf{B}^i = (\mathbf{P}^i)^\top \mathbf{T}^i \mathbf{P}^i = (\mathbf{P}'^i)^\top \mathbf{T}'^i \mathbf{P}'^i$  contains exactly  $\frac{p(p-1)}{2}$  non-zero elements, so it is also the case for  $\mathbf{T}^i$  and  $\mathbf{T}'^i$  which thus represent fully connected graphs. So, from Lemma 6, we deduce that, for each view  $i$ , we have  $\mathbf{P}^i = \mathbf{P}'^i$  and  $\mathbf{T}^i = \mathbf{T}'^i$ , which concludes the proof.

### A.5 Proof of Theorem 4

In the context of shared causal ordering  $\mathbf{P}$ , we prove that, under Assumptions 1 and 3, the decomposition of matrices  $\mathbf{B}^i$  into matrices  $\mathbf{T}^i$  and  $\mathbf{P}$  is unique.

Consider the two sets  $\Theta = (\Sigma^1, \dots, \Sigma^m, \mathbf{P}, \mathbf{T}^1, \dots, \mathbf{T}^m)$  and  $\Theta' = (\bar{\Sigma}^1, \dots, \bar{\Sigma}^m, \bar{\mathbf{P}}, \bar{\mathbf{T}}^1, \dots, \bar{\mathbf{T}}^m)$  that parameterize the same statistical model in Eq. 5, where  $\mathbf{P}$  is some permutation matrix,  $\mathbf{T}^i$  are strictly lower triangular matrices, and  $\bar{\mathbf{P}}$  and  $\bar{\mathbf{T}}^i$  are the particular matrices given by Assumption 3. Note that no assumption on the sparsity of the  $\mathbf{T}^i$  is made. From Theorem 2, we know that  $\Sigma^i = \bar{\Sigma}^i$ .

Assumption 3 amounts to saying that the “reunion” of the  $\bar{\mathbf{T}}^i$  represents a fully connected graph. In other words, if we define the reunion as  $\bar{\mathbf{T}}^U = \sum_{i=1}^m \text{abs}(\bar{\mathbf{T}}^i)$ , where  $\text{abs}$  denotes the element-wise absolute value function, then we are assuming that the strictly lower triangular part of  $\bar{\mathbf{T}}^U$  only has non-zero elements. In a similar way to the definition of  $\bar{\mathbf{T}}^U$ , let us define

$$\bar{\mathbf{W}}^U = \sum_{i=1}^m \text{abs}(\bar{\mathbf{W}}^i)\tag{26}$$

where  $\bar{\mathbf{W}}^i = \mathbf{I} - \bar{\mathbf{P}}^\top \bar{\mathbf{T}}^i \bar{\mathbf{P}}$ . The non-zero elements of  $\bar{\mathbf{P}}^\top \bar{\mathbf{T}}^i \bar{\mathbf{P}}$  are outside of the diagonal, so matrices  $\mathbf{I}$  and  $\bar{\mathbf{P}}^\top \bar{\mathbf{T}}^i \bar{\mathbf{P}}$  contain non-zero elements at different locations. Thus, we have

$$\text{abs}(\mathbf{I} - \bar{\mathbf{P}}^\top \bar{\mathbf{T}}^i \bar{\mathbf{P}}) = \mathbf{I} + \text{abs}(\bar{\mathbf{P}}^\top \bar{\mathbf{T}}^i \bar{\mathbf{P}}).\tag{27}$$

Furthermore, applying  $\bar{\mathbf{P}}$  to the rows and columns of  $\bar{\mathbf{T}}^i$  only shuffles its entries, without modifying their values. So we have

$$\text{abs}(\bar{\mathbf{P}}^\top \bar{\mathbf{T}}^i \bar{\mathbf{P}}) = \bar{\mathbf{P}}^\top \text{abs}(\bar{\mathbf{T}}^i) \bar{\mathbf{P}}.\tag{28}$$

Consequently,

$$\bar{\mathbf{W}}^U = \sum_{i=1}^m \mathbf{I} + \bar{\mathbf{P}}^\top \text{abs}(\bar{\mathbf{T}}^i) \bar{\mathbf{P}} = \sum_{i=1}^m \bar{\mathbf{P}}^\top (\mathbf{I} + \text{abs}(\bar{\mathbf{T}}^i)) \bar{\mathbf{P}} = \bar{\mathbf{P}}^\top (m\mathbf{I} + \bar{\mathbf{T}}^U) \bar{\mathbf{P}}.\tag{29}$$

So, dividing both sides by  $m$  gives

$$\frac{1}{m}\bar{\mathbf{W}}^U = \bar{\mathbf{P}}^\top \left( \mathbf{I} - \left( -\frac{1}{m}\bar{\mathbf{T}}^U \right) \right) \bar{\mathbf{P}} \quad (30)$$

where  $-\frac{1}{m}\bar{\mathbf{T}}^U$  is strictly lower triangular, and its strictly lower triangular part only has non-zero elements.

Next, we apply the same reasoning to the alternative set of parameters, given by  $\mathbf{W}^i = \mathbf{I} - \mathbf{P}^\top \mathbf{T}^i \mathbf{P}$ , and we consider  $\mathbf{W}^U = \sum_{i=1}^m \text{abs}(\mathbf{W}^i)$ . The proof of Theorem 2 already implied that  $\bar{\mathbf{W}}^i = \mathbf{W}^i$  for all  $i$ . Thus, we have  $\bar{\mathbf{W}}^U = \mathbf{W}^U$  and

$$\bar{\mathbf{P}}^\top \left( \mathbf{I} - \left( -\frac{1}{m}\bar{\mathbf{T}}^U \right) \right) \bar{\mathbf{P}} = \mathbf{P}^\top \left( \mathbf{I} - \left( -\frac{1}{m}\mathbf{T}^U \right) \right) \mathbf{P} \quad (31)$$

where  $\mathbf{T}^U$  is defined in a similar way as  $\bar{\mathbf{T}}^U$ , except that its strictly lower triangular part can be sparse. Using Lemma 6 on Eq. 31, we obtain that  $\mathbf{P} = \bar{\mathbf{P}}$ , and thus  $\mathbf{T}^i = \bar{\mathbf{T}}^i$  for all  $i$ . In conclusion, all the sets of DAG decompositions that parameterize the same model are equal, as soon as for one of these decompositions, the reunion of the  $\mathbf{T}^i$  is dense. We conclude that matrices  $\mathbf{P}$  and  $\mathbf{T}^i$  are unique, and thus identifiable in our terminology. This proof also implies that there can be only one matrix  $\bar{\mathbf{P}}$  that fulfills Assumption 3.

## A.6 Proofs of technical lemmas

### A.6.1 Proof of Lemma 5

Consider  $W, W' \in \mathcal{W}$ ,  $K$  a permutation matrix, and  $D$  a diagonal matrix. Suppose that

$$W' = DKW \ . \quad (32)$$

**A permutation inequality on  $K$**  We use the following decompositions from Eq. 19,

$$W = P^\top(I - T)P \ , \quad W' = P'^\top(I - T')P' \ , \quad (33)$$

where  $P, P'$  are permutation matrices and  $T, T'$  are strictly lower triangular matrices. Denote  $L = I - T$  and  $L' = I - T'$ ; these are lower triangular matrices that have unit diagonals. We plug the decompositions into Eq. 32, and get

$$P'^\top L' P' = DKP^\top L P \ . \quad (34)$$

To exploit the structure of the lower triangular matrices  $L$  and  $L'$  and show how they constrain  $K$ , we now switch notations from permutation matrices ( $P, P', K$ ), to their corresponding permutation functions ( $\phi, \phi', \psi$ ). This yields

$$L'_{\phi'(i), \phi'(j)} = D_{ii} L_{\phi(\psi(i)), \phi(j)} \ , \quad \forall i, j \in \llbracket 1, p \rrbracket \ . \quad (35)$$

In particular,  $L'$  has unit diagonal, so

$$1 = L'_{\phi'(i), \phi'(i)} = D_{ii} L_{\phi(\psi(i)), \phi(i)} \ , \quad \forall i \in \llbracket 1, p \rrbracket \ , \quad (36)$$

and  $L$  is lower triangular, so that its non-zero entries must satisfy

$$\phi(i) \leq \phi(\psi(i)) \ , \quad \forall i \in \llbracket 1, p \rrbracket \ . \quad (37)$$

More generally, we can replace  $i$  with  $\psi(i)$ , and so on, and obtain

$$\phi(i) \leq \phi(\psi(i)) \leq \phi(\psi^{(2)}(i)) \leq \dots \quad \forall i \in \llbracket 1, p \rrbracket \quad (38)$$

where the superscript denotes composition and where we can apply the permutation  $\psi$  an arbitrary number of times.

**$K$  must be the identity** Suppose that  $\psi$  is not the identity. We can pick an index  $k \in \llbracket 1, p \rrbracket$  where  $k \neq \psi(k)$ . Because  $\phi$  and  $\psi$  are injective, we can apply them to the inequality any number of times  $n \in \mathbb{N}$  and get

$$\phi(\psi^{(n)}(k)) \neq \phi(\psi^{(n+1)}(k)) \ , \quad (39)$$

which together with Eq. 38 implies

$$\phi(k) < \phi(\psi(k)) < \phi(\psi^{(2)}(k)) < \dots \quad (40)$$

which can be applied any number of times. However, each inequality increases the index by at least one, while the index cannot go above  $p$ . Thus, applying the chain at least  $p$  times, we have a contradiction.

**$D$  must be the identity** Now that we know that  $K = I$ , Eq. 34 becomes

$$P'^\top L' P' = D(P^\top L P) \ . \quad (41)$$

The matrix  $P'^\top L' P'$  has a diagonal of ones and so too does  $P^\top L P$ . It follows that  $D = I$ . This concludes the proof of the Lemma.

### A.6.2 Proof of Lemma 6

From the equality  $\mathbf{P}^\top \mathbf{T} \mathbf{P} = \mathbf{P}'^\top \mathbf{T}' \mathbf{P}'$ , we deduce that

$$\mathbf{T} = \tilde{\mathbf{P}}^\top \mathbf{T}' \tilde{\mathbf{P}} , \quad (42)$$

where  $\tilde{\mathbf{P}} = \mathbf{P}' \mathbf{P}^\top$  is the permutation matrix represented by function  $\phi$ , which is defined such that:  $\forall k \in \llbracket 1, p \rrbracket$ ,  $\tilde{\mathbf{P}}_{k, \phi(k)} = 1$  and  $\forall l \neq \phi(k)$ ,  $\tilde{\mathbf{P}}_{k, l} = 0$ . Using the notation  $\phi$  instead of  $\tilde{\mathbf{P}}$ , Eq. 42 can be rewritten as,  $\forall k, l \in \llbracket 1, p \rrbracket$ ,

$$\mathbf{T}_{k, l} = \mathbf{T}'_{\phi(k), \phi(l)} . \quad (43)$$

We proceed by a proof by contradiction: assume that  $\tilde{\mathbf{P}} \neq \mathbf{I}$ . As a consequence, there exists an index  $k$  such that  $\phi(k) \neq k$ . Let us fix such an index as  $k$ . We can assume without loss of generality that

$$\phi(k) > k , \quad (44)$$

otherwise we just have to invert signs and switch rows and columns in the following. By assumption, the strictly lower triangular part of  $\mathbf{T}$  only has non-zero elements, so we have

$$\mathbf{T}_{\phi(k), k} \neq 0 . \quad (45)$$

Yet, from Eq. 43, we know that  $\mathbf{T}_{\phi(k), k} = \mathbf{T}'_{\phi(\phi(k)), \phi(k)}$  and all the non-zero elements of  $\mathbf{T}'$  are in its strictly lower triangular part, which implies

$$\phi(\phi(k)) > \phi(k) . \quad (46)$$

This logic can be applied repeatedly as in the preceding lemma's proof, and we see that

$$\phi(k) < \phi^{(2)}(k) < \phi^{(3)}(k) < \dots . \quad (47)$$

Now, this leads to an infinite strictly increasing sequence, which is contradictory since the index cannot grow greater than  $p$ . So,  $\tilde{\mathbf{P}} = \mathbf{I}$ , which means that  $\mathbf{P}' \mathbf{P}^\top \mathbf{P} = \mathbf{P}$ , and thus, using the orthogonality of  $\mathbf{P}$ ,

$$\mathbf{P}' = \mathbf{P} . \quad (48)$$

It also follows that  $\mathbf{T}' = \mathbf{T}$ , which concludes the proof of Lemma 6.

## B Additional experiments

### B.1 Additional simulations

In the two following simulations, we study a third version of the MICaDo algorithm where the multi-view ICA algorithm ShICA [20] is replaced with MVICA [21]. This version is called MICaDo-MVICA and is displayed in purple. Although MVICA was not specifically designed to handle Gaussian disturbances, experiments proved that it was quite robust against Gaussianity [21].

**Multiple causal orderings** We explore in this paragraph the case where causal orderings are view-specific. To do so, we use the experiment setup of Fig. 1 but use multiple matrices  $\mathbf{P}^i$  instead of a shared matrix  $\mathbf{P}$  and we display the results in Fig. 4. One can observe that this setting is not favourable to MultiGroupDirectLiNGAM [24], which still tries to estimate a shared causal ordering, hence the bad performance of the red curve. On the other hand, MICaDo-ML still achieves state-of-the-art results, even when estimating multiple causal orderings. The results of MICaDo-ML, MICaDo-J, and ICA-LiNGAM [26] are comparable to the ones in Fig. 1. In addition, we can observe that MICaDo-MVICA seems to achieve the best results in the pure non-Gaussian scenario, very close to MICaDo-ML and ICA-LiNGAM, but it fails when all disturbances are Gaussian. Interestingly, we can see that its performance increases as the number of samples increases. This experiment confirms that MICaDo-ML is the only one of the studied algorithms that performs well in all three scenarios.

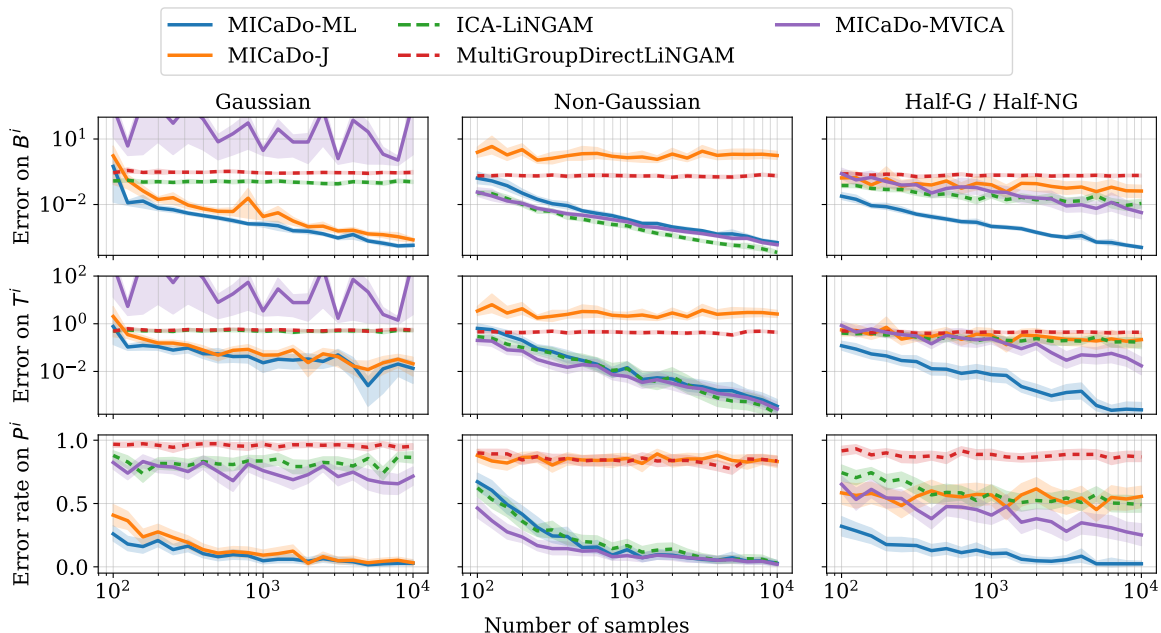


Figure 4: Separation performance of ICA-LiNGAM [26], MultiGroupDirectLiNGAM [24] and three versions of our method in the *multiple causal orderings* context and while varying the number of samples. Left column: all disturbances are Gaussian. Middle column: all disturbances are non-Gaussian and the noise variances are equal. Right column: half of the disturbances are Gaussian and the other half are non-Gaussian. There are three different metrics: the  $\ell_2$ -distance between true and estimated causal effect matrices  $\mathbf{B}^i$  (upper row), the  $\ell_2$ -distance between true and estimated matrices  $\mathbf{T}^i$  (middle row), and the rate of failed estimated causal orderings  $\mathbf{P}^i$  over all repetitions (lower row; lower is better). We used 50 different seeds.

**Varying noise level** It is well-known in ICA theory that algorithms find it increasingly difficult to estimate components as noise increases. Since our method relies on multiview ICA estimation, studying how performance varies when noise level increases is important. In Fig. 5, we reproduce the simulation of Fig. 1 and 4 but set the number of samples  $n$  to 1000 and vary the noise level (previously set to 1) from  $10^{-2}$  to  $10^2$ . As in Fig. 1, we use the shared causal ordering setting.

We can observe that MICaDo-ML achieves the best results (just ahead of MICaDo-J) when disturbances are Gaussian and the noise level is between  $10^{-1}$  and 10. The drop in performance of MICaDo-ML

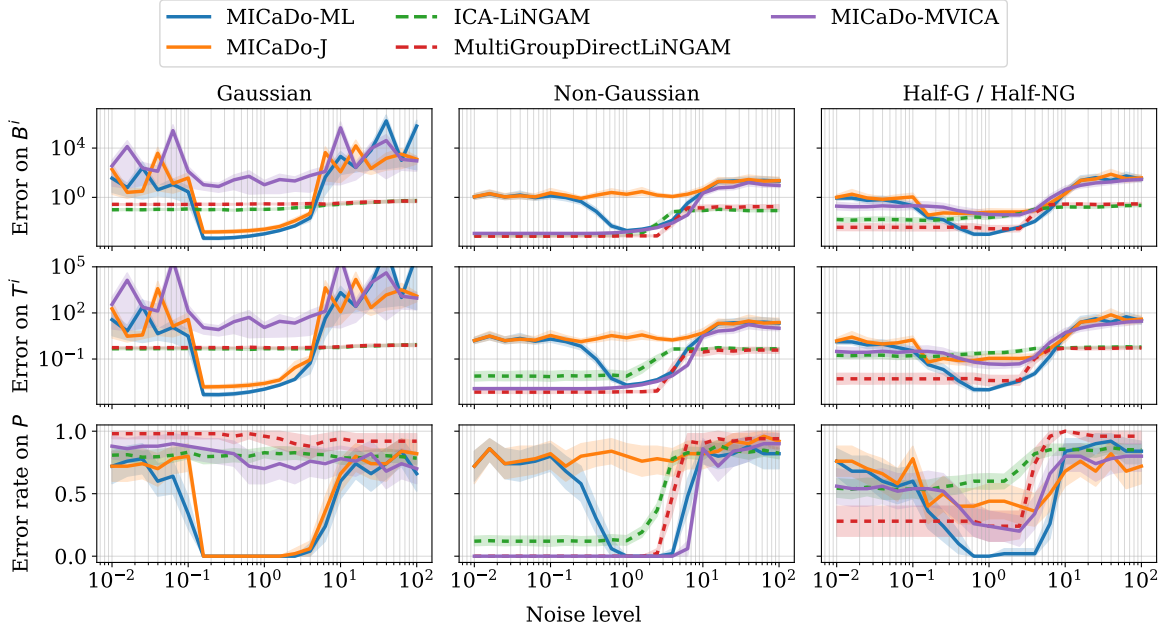


Figure 5: Separation performance of ICA-LiNGAM [26], MultiGroupDirectLiNGAM [24] and three versions of our method in the shared causal ordering context and while varying the noise level. The three scenarios and three metrics are the same as in Fig. 1 and 4.

and MICaDo-J when the noise level goes below  $10^{-1}$  can probably be explained by the reduction in noise diversity. Below  $10^{-1}$  and above 10, none of the methods gives good results.

In the context of non-Gaussian disturbances, MICaDo-MVICA and MultiGroupDirectLiNGAM [24] outperform the other methods, especially when the noise level is lower than 1. The original ICA-LiNGAM [26] produces decent results, whereas MICaDo-ML is only competitive when the noise level is in  $[1, 10]$  and MICaDo-J is bad. When the noise level exceeds 10, none of the methods retrieve the parameters.

When half of the disturbances are Gaussian and the other half are non-Gaussian, results are more mixed. We can observe that MICaDo-ML achieves the best results when the noise level is close to 1 (i.e. sources and noises are of similar orders) but MultiGroupDirectLiNGAM outperforms other methods as soon as the noise level is below a threshold somewhere in  $[10^{-1}, 1]$ . As for the other scenarios, none of the methods give good results when the noise goes beyond 10.

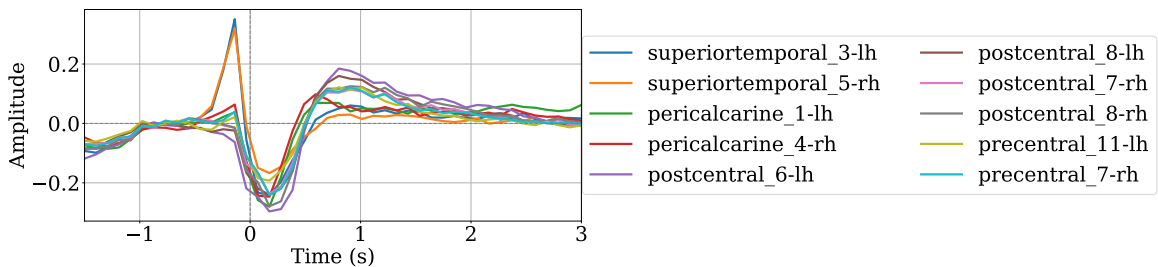


Figure 6: Example of time series obtained after the preprocessing. We averaged the data across subjects and trials, resulting in 10 time series, one for each brain region.

## B.2 Additional experiments on real data

In the following, we extend the experiments conducted in Section 6. First of all, Fig.6 represents the typical time series obtained after the preprocessing. For visualization purposes, we averaged these time series across subjects and trials. We see a peak happening before the button press (at  $t = 0$  s) in the “superiortemporal” auditory regions, due to the stimulus. We also see a clear rebound effect in the motor regions, as the corresponding time series drop around  $t = 0$  s (as the beta waves desynchronize) and then rise from  $t = 0.3$  s (as they synchronize again). This figure also gives the names of the 10 selected parcels.



Figure 7 shows additional brain plots, as a supplement to Fig. 2. For each of the six runs, we randomly selected 50% of the participants and applied MICaDo-ML to their data. The same observations apply to the four additional plots, namely that many arrows point from the motor cortex of one hemisphere to the motor cortex of the other hemisphere.

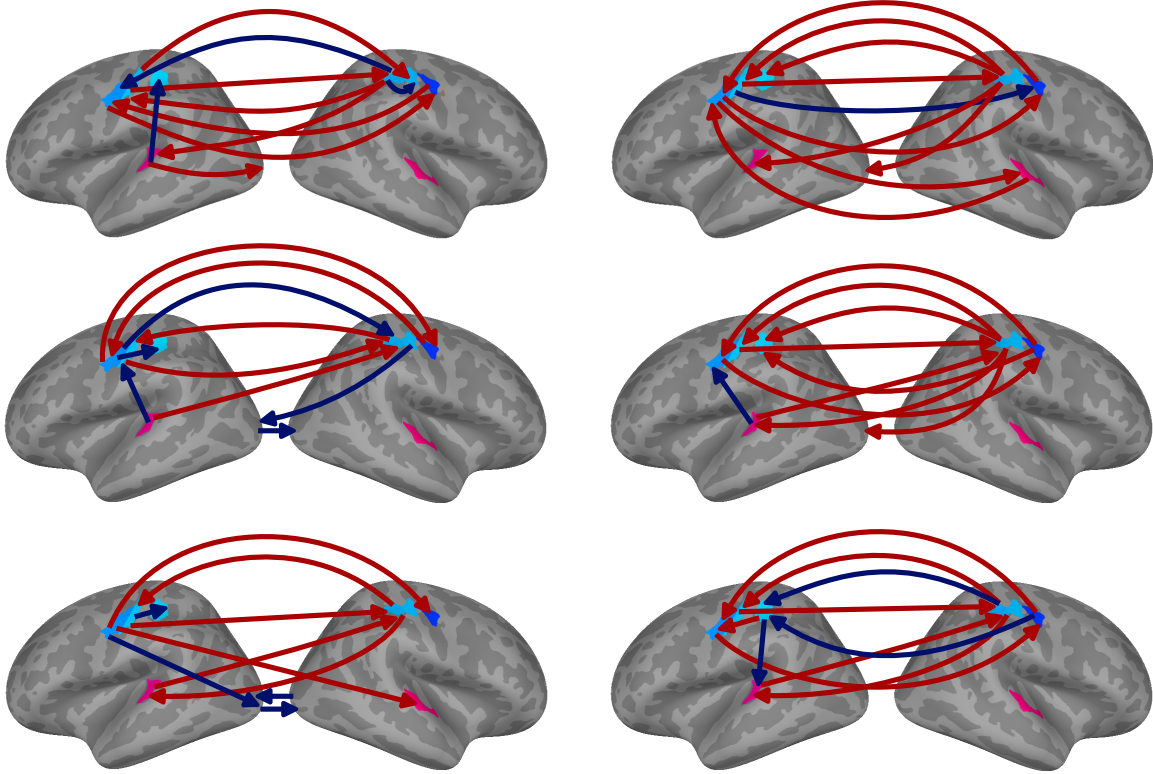


Figure 7: Top ten most important causal effects on six different runs. Each run was performed on the data of 49 randomly chosen subjects. We took the median of the causal effect matrices and picked the 10 highest entries in absolute value. Red arrows represent positive effects and blue arrows negative effects. The two runs at the top correspond to the ones in Fig. 2.

Fig. 8 shows the Pearson correlations between the median matrices obtained for each of the 50 runs. More specifically, for each run, we computed the element-wise median of the  $B^i$  matrices, and then we calculated the Pearson correlation between flattened median matrices, for all pairs of runs. This procedure gives an average correlation of 0.39. This result tends to show that the medians of the  $B^i$  matrices are consistent across runs.

Finally, Fig. 9 shows the Spearman's rank correlation matrix whose entries are used in Fig. 3. This matrix studies the correlations between the 50 estimated causal orderings. We can see that, apart from a few particular runs (2, 16, 35, and 47), the orderings are often positively correlated.

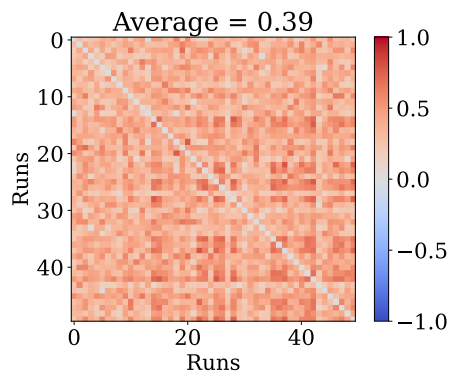


Figure 8: Pearson correlations between the flattened median causal effect matrices obtained for each of the 50 runs.

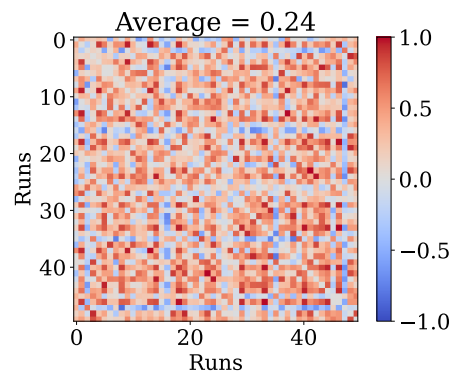


Figure 9: Spearman's rank correlations between estimated orderings  $\mathbf{P}$ . This matrix corresponds to the histogram in Fig. 3.